Numerical analysis of steady and transient processes in a directional solidification system

Ting-Kang Lin, Chung-Hao Lin and Ching-Yao Chen[*]

Department of Mechanical Engineering, National Chiao Tung University, Taiwan, R.O.C.

Abstract. Manufactures of multi-crystalline silicon ingots by means of the directional solidification system (DSS) is important to the solar photovoltaic (PV) cell industry. The quality of the ingots, including the grain size and morphology, is highly related to the shape of the crystal-melt interface during the crystal growth process. We performed numerical simulations to analyze the thermo-fluid field and the shape of the crystal-melt interface both for steady conditions and transient processes. The steady simulations are first validated and then applied to improve the hot zone design in the furnace. The numerical results reveal that, an additional guiding plate weakens the strength of vortex and improves the desired profile of the crystal-melt interface. Based on the steady solutions at an early stage, detailed transient processes of crystal growth can be simulated. Accuracy of the results is supported by comparing the evolutions of crystal heights with the experimental measurements. The excellent agreements demonstrate the applicability of the present numerical methods in simulating a practical and complex system of directional solidification system.

1. Introduction

The multi-crystalline-silicon based solar cell has the highest market share in the worldwide production of photovoltaic cells. Advanced manufacturing procedure of the multi-crystalline silicon ingot is strongly desired to reduce the cost, and to enhance the quality of the photovoltaic cells. The performance of the photovoltaic cell can be affected by the grain size and the morphology of the multi-crystalline silicon. Larger and more uniform grains of the multi-crystalline silicon improve the conversion efficiency of the solar cell (Fujiwara *et al*. 2006). It has been understood that the formation of the grains is highly related to the shape of the crystal-melt interface. Directional solidification system (DSS) is a cost-effective method for the production of the multi-crystalline silicon ingot (Newman 1996). Intensive works toward the heat transfer and impurity distributions to improve the quality of the ingot had been presented. Nakano *et al*. (2013) used the top and side heaters to control the oxygen concentration in the silicon melt. They presented that the oxygen concentration in the melt by the side heating system is lower than that

---

*Corresponding author, Professor, E-mail: chingyao@mail.nctu.edu.tw

only by the top heating system. Shur *et al*. (2011) applied two different cooling methods to improve the ingot quality. Zhang *et al*. (2011) proposed that enhancement of the G/V value, in which G is the temperature gradient near the interface, and V is the growth rate, may also improve quality of the ingot. The effect of argon flow and furnace pressure to the flow field and the thermal distribution in the melt region as well as to the impurities transport in the DSS furnace had also been investigated (Li *et al*. 2011a, b). Teng *et al*. (2010) studied the distributions of the carbon concentration in the melt and in the silicon crystal both by the experiments and the numerical simulations. Effects of the inlet pressure and the installation of an additional gas flow guiding device to the impurity distribution in the silicon melt had also been evaluated (Teng *et al*. 2011, 2012, 2013). Devulapalli and Kulkarni (2009) carried out the simulations of unsteady solidification process for the improvement of the grain boundaries and dislocations of the ingot. Miyazawa *et al*. (2008, 2009) investigated how the material properties and the shape of a crucible affect the profile of the interface. They found that the thermal conductivity of the crucible plays a significant role on the melt-crystal interface. Calculations of the crystallization front by 2-dimensional and 3-dimensional models were performed by Kuliev *et al*. (2007). In the early stage of the growth process, slightly fast nucleation rate near the quartz crucible is desired to increase the crystallization rate. It implies that a less concave solid-liquid interface near the quartz crucible is better. In the middle stage, however, the solid-liquid interface requires more concave near the quartz crucible because of a desired slower crystallization rate. Otherwise, the growth of the grains will be started from the quartz crucible to the center of the ingot. It is noticed that these phenomena affect the ingot quality directly. According to the silicon crystal growth principle (Shimura 1989), the crystallization rate and the shape of crystal-melt interface shape are highly related to the balance of thermal flux between the crystal and the melt. Therefore, the control of the thermal dissipation is crucial to the crystallization rate and the interface shape. The thermal dissipation can be achieved by modifying configurations of the furnace.

In this study, we aim to carry out more challenging simulations of transient crystal growth processes in the DSS furnace by means of the software package of CGSim. To achieve the aims, steady simulations are first performed to realize the detailed distributions of flows and temperatures as well as the profile of crystal-melt interface. To modify the furnace configuration for a better profile of crystal-melt interface, installing a guiding plate to control the argon flow around the side heaters is also tested. To improve the accuracy of transient simulations, results of steady simulations at early times are taken as initial conditions. The numerical simulations are validated by the corresponding experimental measurements. The effects of the thermal dissipation to the corresponding interface shape will be focused.

2. Physical model and computational method

A schematic of the original DSS furnace used in this study for the growth of the multi-crystalline silicon is presented in the left of Fig. 1. The modified furnace with an additional guiding plate (marked as component 15) is also displayed in the right of Fig. 1. When the movable insulator (component 4) is lifted, the silicon crystal starts to grow (or solidify) from the bottom of the quartz crucible (component 10) because of heat loss to the furnace wall (component 13). In order to numerically investigate the processes of crystal solidifications, the silicon melt and the argon gas are considered as a Newtonian fluid and an ideal gas, respectively. In addition, all radiative surfaces are assumed to be diffuse-gray. The steady governing equations in the fluid are

given as

$$\nabla \cdot (\rho \vec{u}) = 0 \tag{1}$$

$$(\vec{u} \cdot \nabla)\rho \vec{u} = \nabla P + \nabla \cdot \vec{\vec{\tau}} + (\rho - \rho_0)\vec{g} \tag{2}$$

$$\nabla \cdot (\rho C_p \vec{u} T) = \nabla \cdot (k \cdot \nabla T) \tag{3}$$

where ρ, u, P, $\vec{\vec{\tau}}$, g, ρ_0, T, C_p, k are the fluid density, the velocity, the furnace pressure, the stress tensor, the gravity, the reference density, the temperature, the heat capacity, and the thermal conductivity, respectively. In the solid, the heat transfer Eq. (3) becomes

$$\nabla \cdot (k \cdot \nabla T) + S = 0 \tag{4}$$

where S is the source term generated by the side (component 2) and top (component 1) heaters.

The boundary condition on the gas-melt surface which represents the balance of shear stresses is given by

$$(\mu \frac{\partial \vec{u}}{\partial n})_m = (\mu \frac{\partial \vec{u}}{\partial n})_{gas} + \frac{\partial \sigma_m}{\partial T} \frac{\partial T}{\partial \tau}, \tag{5}$$

where μ, n and σ_m are the dynamic viscosity, the normal direction of the interface, and the surface tension of the silicon melt, respectively. The last term of the right hand side is the Marangoni effect, and τ stands for the orthogonal direction tangential to the gas-melt surface. On the interface between two opaque blocks, equations balancing the temperature and heat are described by

$$T_{block1} = T_{block2}, \tag{6}$$

$$(k \frac{\partial T}{\partial n})_{block1} = (k \frac{\partial T}{\partial n})_{block2}. \tag{7}$$

If the interface is between opaque and transparent blocks, the heat balance equation is modified as

$$(k \frac{\partial T}{\partial n})_{opaque} = (k \frac{\partial T}{\partial n})_{transparent} + \sigma \varepsilon T^4 - q_i^{in}, \tag{8}$$

where σ and ε are the Stefan-Boltzmann constant and the emissivity, respectively. The last term of the right hand side is the total radiative flux incoming to the surface i. In addition, the Stefan condition is used to calculate of the crystallization rate on the solid-liquid interface, so that

$$\rho_s u_s \Delta H = [(k \frac{\partial T}{\partial n})_m - (k \frac{\partial T}{\partial n})_s] \tag{9}$$

where ρ_s, ΔH, and u_s are the density of the silicon crystal, the latent heat, and the local crystallization rate normal to the interface, respectively.
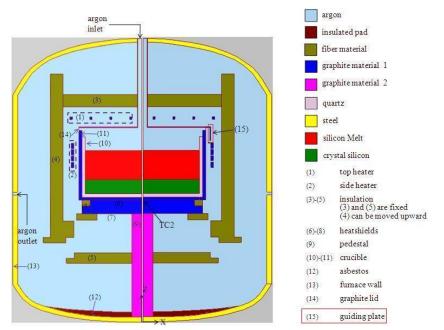
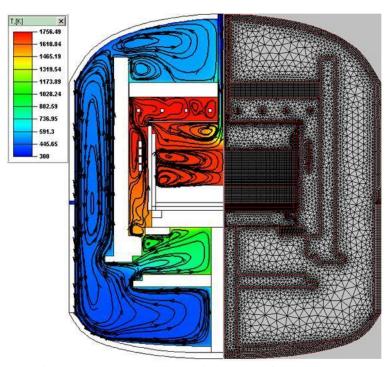Fig. 1 Schematics of simulated DSS furnaces without (left) and with (right) a guiding plate (component 15)

Fig. 2 Shown in the right is the mesh applied to simulate the furnace without a guiding plate at a crystal height of *H*=105 mm. Correspondent distributions of temperate and flow fields in all fluid regions, i.e., including gases and melts, are demonstrated in the left. Silicon crystal inside the quartz crucible is displayed in blank, where temperature is lower than 1685 K. Interface between crystal and melt appears convex and concave near the central region and wall of crucible, respectively

Table 1 Values of physical properties used in simulations (STR Group 2012c)

Material	Property	Value
Argon	heat conductivity (W/m K)	$0.01+2.5\times10^{-5}T$
	heat capacity (J/kg K)	521
	dynamic viscosity (Pa s)	$8.466e-6+5.365e-8T^2-8.682T^4$
	emissivity	0.8
Graphite material 1	heat conductivity (W/m K)	$146.9-0.1777T+1.27e-4T^2-4.69e-8T^3+6.665e-12T^4$
	heat capacity (J/kg K)	710
	density (kg/m^3)	1950
	emissivity	0.8
Graphite material 2	heat conductivity (W/m K)	105
	heat capacity (J/kg K)	1000
	emissivity	0.8
Quartz	heat conductivity (W/m K)	4
	heat capacity (J/kg K)	1232
	density (kg/m^3)	2650
	emissivity	0.85
Silicon crystal	heat conductivity (W/m K)	$110.6-0.1507T+0.0001T^2+4.01e-8T^3+$ $5.668e-12T^4$
	heat capacity (J/kg K)	1000
	density (kg/m^3)	2530
	emissivity	$0.9016-0.0003T$
Silicon melt	heat conductivity (W/m K)	66.5
	heat capacity (J/kg K)	915
	density (kg/m^3)	$3194-0.3701T$
	dynamic viscosity (Pa s)	0.0008
	emissivity	0.3
	latent heat (J/kg)	1800000
	surface tension (N/m)	0.7835
	melting point (K)	1685
Insulation pad	heat conductivity (W/m K)	0.35
	heat capacity (J/kg K)	600
	emissivity	0.7
Fiber	heat conductivity (W/m K)	0.44
	heat capacity (J/kg K)	2000
	density (kg/m^3)	170
	emissivity	0.85

Numerical mesh, as shown in the right of Fig. 2, is constructed by both the structured and unstructured grids with 27,146 computational cells. Axis-symmetric domain is assumed in the simulations. To capture the detailed local distributions of velocities and temperatures, the grids are

refined at regions on the solidification interface and near the quartz crucible. The above governing equations associated with the boundary conditions are solved by the commercial software CGSim. CGSim is based on the finite volume method and has been successfully applied in numerous early studies for crystal growth (Black *et al.* 2012, Chen and Dai 2012, Chen *et al.* 2011, Demina and Kalaev 2011, Lin *et al.* 2011, Noghabi *et al.* 2011, Noghabi *et al.* 2013, Teng *et al.* 2011, Teng *et al.* 2012). The physical properties used in this study are presented in Table 1.

3. Results and discussion

3.1 Steady simulations without/with a guiding plate

A series of steady simulations at different crystal heights of *H*=18 mm, 105 mm, 204 mm, and 248 mm in an original furnace without a guiding plate, as shown in the left of Fig. 1, are first performed. Detailed flow patterns and the temperature distributions in the entire fluid region, including the argon gas and silicon melts, for a representative case of *H*=105 mm are depicted in the left of Fig. 2. To illustrate the entire thermo-fluid field, four main regions are categorized, such as (I) the outer argon flow between the furnace wall and the insulators, (II) inner argon flow between the insulators and crucible, (III) argon flow within the crucible and (IV) the crystal melt inside the crucible. In the region (I), argon tends to flow clockwise when argon exits the furnace through the opened gap. A large vortex (or a vortex ring in a three-dimensional configuration) is observed. Due to the insulation, the temperature is significantly lower in this region (I). Since the main function of this region is a vent, the effects to the growth of crystal are generally less important. The temperature is much higher in the region (II), where the heaters are placed. Even the overall pattern of argon flow is downward to exit from the gap between the insulators and crucible, the local circulations around the heaters are induced by the natural convection. This region (II) is directly near the crucible wall which covers across the solid-fluid interface, so that the flow fields as well as the effects of heat transfer are expected to be crucial to the phenomenon of solidification. More detailed discussion regarding the local fields in this region (II) is emphasized in a latter paragraph. In region (III), the argon gas enters/exits through the central inlet/upper-corner outlet. A reverse circulation of argon flow occurs due to a sudden expansion in space. The temperature in this reverse circulation area is lower because of continuous supply of cool argon flow which is farther away from the heaters. The melt flow in the region (IV) also influences the processes of crystal growth importantly. It is affected by coupled factors, such as (1) the higher temperature generated by the heaters on the side, (2) lower temperature on the bottom caused by the lift of insulators and no-slip velocity by the solid crystal, and (3) heat convection and shear induced by the argon flow on the top. Two counter-rotating vortexes are observed. The formation of such vortexes plays a main role in determining the profile the crystal interface, as well as the distributions of relevant chemical components, which are not considered in the present study. Affected by the vortex, crystal-melt interface appears convex and concave near the central region and crucible wall, respectively. The overall patterns of the simulations are generally consistent with results presented in Teng *et al.* (2011). To further validate the simulated results, direct comparisons with the experimental measurements of temperature at a position beneath the crucible (STR Group 2012) for different silicon height of *H*=105 mm, 204 mm, and 248 mm are shown in Table 2. Excellent agreements are obtained to ensure the credibility of simulations with the insignificant errors around 3 percentages.
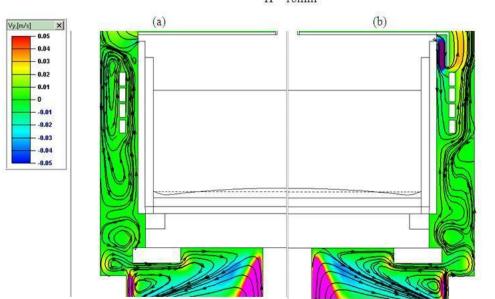
H = 18mm

Fig. 3 Streamlines around the side heaters at the crystal height of *H*=18 mm. Shown in the right and left are cases with and without a guiding plate, respectively. A counterclockwise vortex stretches to surround nearly the entire crucible without the guiding plate. On the other hand, installation of the additional guiding plate suppresses the strength of vortex
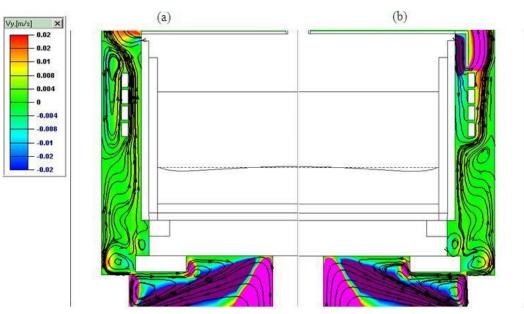
H = 105mm

Fig. 4 Streamlines around the side heaters at a crystal height of *H*=105 mm. Shown in the right and left are cases with and without a guiding plate, respectively. Shielded by the guiding plate, most of the argon is prevented to flow through the gap between heaters and crucible wall. Stronger upward covection near the interface region is observed for the case with a guiding plate

Table 2 Comparisons of temperatures by the present simulations and the experimental measurements at various silicon crystal heights

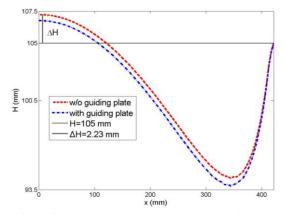| Silicon crystal height (H)	H=105 mm	H=204 mm	H=246 mm
Measured temperature (private communications)	1411.85 K	1368.05 K	1357.85 K
Calculated temperature	1367.6 K	1326.9 K	1318.4 K
Error	3.13%	3%	2.91%

Fig. 5 The crystal-melt interfaces for the cases with and without a guiding plate at the height of H=105 mm. Positions x=0 and 421.5 mm represent center of the crystal and wall the quartz crucible, respectively. The installation of guiding plate enhances the concaveness of interface near the wall region, which is desired for a better crystal growth

As mentioned in the previous paragraph, the crystal-melt interface might be directly affected by the thermo-fluid distribution in the region (II), so that modification of thermo-fluid distribution in this region is possible to improve the profile of solidification. The idea is installing an additional guiding plate connected with the graphite lid, as the component 15 shown in the right of Fig. 1. Figs. 3 and 4 presented the comparisons of vertical-velocity fields in this region (II) between the cases with and without the guiding plate at two stages of crystal growth process, e.g., an early stage of H=18 mm and a middle stage of 105 mm, respectively. It is noticed that the temperature is lower within the region of solid crystal, so that prominent natural convection might be confined in the area of adjacent to the melt. At an early stage of crystal growth when the interface is located on a lower position of H=18 mm, the counterclockwise vortex stretches to surround of the entire crucible without the guiding plate, as shown in the left of Fig. 3. Similar situation is observed at a middle stage of H=105 mm, as shown in the left of Fig. 4. The only difference is the length of counterclockwise vortex is compressed due to the lift of crystal-melt interface. Because of a shorter depth to accommodate the vortex, the circulating strength between the heaters and crucible wall is enhanced. This indicates that, without the guiding plate, the flow fields vary greatly through the entire process of crystal growth, e.g., Figs. 3(a) and 4(a). On the other hand, installation of the additional guiding plate suppresses the strength of vortex as shown in the left of Figs. 3(b) and 4(b). The flow pattern appears more uniformly toward the vertical orientation. A less prominent vortex which merely affects heaters is induced. Additionally, because the argon flow between the heaters and crucible wall is shielded by the plate, movement of the argon flow is
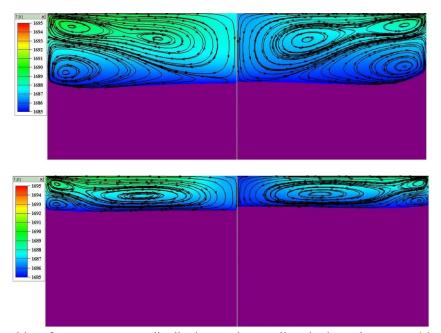
Fig. 6 Crystal interfaces, temperature distributions and streamlines in the melts at $t=t_0+4$ hrs (top) and t_0+12 hrs (bottom) for conditions A (constant growth rate) and B (constant TC2 temperate), which are shown in the left and right columns, respectively. The purple regions are the solidified crystals. When the height of crystal has grown higher to further compress the melt region, the development of the lower vortex adjacent to the solid is confined, and reduces the concaveness of the interface near the wall. The interface appears flatter at a later time, e.g., $t=t_0+12$ hrs shown in the bottom row
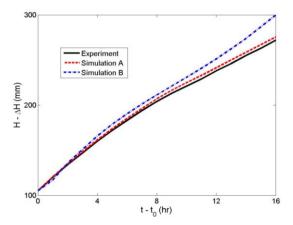

Fig. 7 Evolutions of crystal height predicted by the transient simulations and the experimental measurement. The starting time t_0 of simulations is at H=105 mm. The calculated heights are adjusted by the initial deviation ΔH caused by the non-flat interface shown in Fig. 5. Simulations A and B are under conditions of fixed crystal growth rate and temperature at TC2 position (displayed in Fig. 1), respectively. Excellent predictions are obtained in both simulations

less significant. In general, the overall flow patterns during different stages of growth, e.g., Figs. 3(b) and 4(b), are not altered significantly with the presence of the guiding plate. It clearly

indicates that the installation of such a guiding plate can effectively maintain a relatively more steady flow field in the region (II). It is known that, because of a desired slower crystallization rate at the middle stage of growth process, a more concave crystal-melt interface near the wall of crucible is better. By inspecting the area near the interface, it can be observed that local convections are much stronger in the case with guiding plate than without guiding plate, e.g., more concentrated upward streamlines in Fig. 4(b) compared with Fig. 4(a). As a result, higher amount of heat generated by the heaters can be transferred to the interface area and slow down crystallization rate. The comparison of the crystal-melt interfaces between the cases with and without the guiding plate for the silicon crystal height H=105 mm is shown in Fig. 5. It is noticed the prominence of the concaveness is enhanced by the presence of the plate to justify the installation of such a guiding plate.

3.2 Simulations of transient crystal growth processes

After reliable steady simulations are achieved in the previous section, more practical simulations of transient growth processes are performed. To start the transient simulations, initial conditions are required. The steady state solution of H=105 mm, which is shown in the left of Fig. 2, is taken as the initial condition as $t=t_0$. The unsteady governing equations will be solved numerically to advance in time. Two distinct control mechanisms are applied to analyze the transient growth processes; condition (A): a fixed crystallization rate, and condition (B): a fixed temperature at point TC2 shown in Fig. 1. The transient phenomena regarding the profiles of crystal-melt interface and the flow fields within the melts are focused. Furthermore, evolutions of the average crystal heights will be compared with the actual experimental measurements.

The results are shown in Fig. 6 for 4 hours ($t_1=t_0+4$ hrs) and 12 hours ($t_2=t_0+12$ hrs) after the initial condition. At $t=t_1$, the height of crystal grows significantly compared to the initial time at $t=t_0$ (shown in Fig. 2), so that amount of the melt is reduced. Due to a narrower space of the melts, the dual vortexes are compressed. The height and concaveness of the crystal-melt interface is slightly larger in condition (B). Similar trend keeps evolving at a later time $t=t_2$ when the height of crystal has grown up to further compress the melt region. Due to constraint of the no-slip velocity in the crystal-melt interface, the development of the lower vortex near the solid is further confined. The weak strength of this lower vortex reduces the concaveness of the interface near the wall. The interface is more horizontal compared to earlier stages. Even the heights of the crystal and flow fields in the melts show slight differences in the two simulations, the overall patterns and trends are consistent with both control mechanisms.

To summarize the simulated results, the heights of crystal are compared with the experiments. The position measured in the experiments is at the center of the interface. Since the whole interface is not perfectly flat, the actual height of crystal is slightly higher than prescribed condition, in which the deviation is denoted as ΔH as shown in Fig. 5. As a result, the comparisons should be made by deducting the deviation, and shown in Fig. 7. The prediction by condition (A) agrees excellently with the experiments, while slightly over-growth is obtained by condition (B). The good agreements vindicate the applicability of transient numerical simulations.

4. Conclusions

The crystallization rate and the interface shape, which are crucial factors in the productions of

multi-crystalline silicon ingot by the directional solidification system, are highly related to the dissipation of heat. Detailed understandings of the thermo-fluid fields in the furnace are essential for better processes of crystal growth. The control of the thermo dissipation can be carried out by modifying the configuration of hot zone in the furnace. In the present study, the direct numerical simulations in the DSS furnace are performed by CGSim, a specialized numerical package for crystal growth. A series of steady state simulations are first validated by excellent agreements with the experimental measurements of temperatures. Afterward, the package is applied to search for better designs in the hot zone. The results confirm that the flow fields can be effectively controlled by installing a guiding plate. By this installation, better shape of the crystal-melt interface can be obtained. Furthermore, a more practical task to simulate the transient processes in the whole DSS furnace is performed. The transient simulations are capable to capture detailed melt flows and crystal-melt interfaces at different times. The credibility of the transient simulations is also supported by the good agreements in predicting the evolution of crystal heights with the experimental measurements.

References

Black, A., Medina, J., Pineiro, A. and Dieguez, E. (2012), "Optimizing seeded casting of mono-like silicon crystals through numerical simulation", *J. Cryst. Grow*., **353**(1), 12-16.

Chen, J.C., Teng, Y.Y., Wun, W.T., Lu, C.W., Chen, H.I., Chen, C.Y. and Lan, W.C. (2011), "Numerical simulation of oxygen transport during the CZ silicon crystal growth process", *J. Cryst. Grow*., **318**(1), 318-323.

Chen, L. and Dai, B. (2012), "Optimization of power consumption on silicon directional solidification system by using numerical simulations", *J. Cryst. Grow*., **354**(1), 86-92.

Devulapalli, B. and Kulkarni, M.S. (2009), "Modeling multi-crystalline silicon growth in directional solidification systems", *ECS Trans*., **18**(1), 1023-1029.

Demina, S.E. and Kalaev, V.V. (2011), "3D unsteady computer modeling of industrial scale Ky and Cz sapphire crystal growth", *J. Cryst. Grow*., **320**(1), 23-27.

Fujiwara, K., Pan, W. and Sawada, K. (2006), "Directional growth method to obtain high quality polycrystalline silicon from its melt", *J. Cryst. Grow*., **292**(2), 282-285.

Kuliev, A.T., Durnev, N.V. and Kalaev, V.V. (2007), "Analysis of 3D unsteady melt flow and crystallization front geometry during a casting process for silicon solar cells", *J. Cryst. Grow*., **303**(1), 236-240.

Lin, C.H., Chen, P.W. and Chen, C.Y. (2011), "Simulations of silicon Cz growth in a cusp magnetic field", *Magnetohydr*., **47**(1), 17-28.

Li, Z.Y., Liu, L., Ma, W.C. and Kakimoto, K. (2011a), "Effects of argon flow on heat transfer in a directional solidification process for silicon solar cells", *J. Cryst. Grow*., **318**(1), 298-303.

Li, Z.Y., Liu, L., Ma, W.C. and Kakimoto, K. (2011b), "Effects of argon flow on impurities transport in a directional solidification furnace for silicon solar cells", *J. Cryst. Grow*., **318**(1), 304-312.

Miyazawa, H., Liu, L. and Kakimoto, K. (2008), "Numerical analysis of influence of crucible shape on interface shape in a unidirectional solidification process", *J. Cryst. Grow*., **310**(6), 1142-1147.

Miyazawa, H., Liu, L. and Kakimoto, K. (2009), "Numerical investigation of the influence of material property of a crucible on interface shape in a unidirectional solidification process", *Cryst. Grow. Des*., **9**(1), 267-272.

Newman, R.C. (1996), "Light impurities and their interactions in silicon", *Mater. Sci. Eng.: B*, **36**(1-3), 1-12.

Noghabi, O.A., M'Hamdi, M. and Jomâa, M. (2011), "Effect of crystal and crucible rotations on the interface shape of Czochralski grown silicon single crystals", *J. Cryst. Grow*., **318**(1), 173-177.

Nakano, S., Gao, B. and Kakimoto, K. (2013), "Relationship between oxygen impurity distribution in

multi-crystalline solar cell silicon and the use of top and side heaters during manufacture", *J. Cryst. Grow*., **375**, 62-66.

Noghabi, O.A., Jomâa, M. and M'hamdi, M. (2013), "Analysis of W-shape melt/crystal interface formation in Czochralski silicon crystal growth", *J. Cryst. Grow*., **362**, 77-82.

Shimura, F. (1989), "Semiconductor silicon crystal technology", Academic Press, San Diego, U.S.A.

Shur, J.W., Kang, B.K., Moon, S.J., So, W.W. and Yoon, D.H. (2011), "Growth of multi-crystalline silicon ingot by improved directional solidification process based on numerical simulation", *Sol. Energy Mater. Sol. Cell*., **95**(12), 3159-3164.

STR Group (2012), *Private Communications*.

Teng, Y.Y., Chen, J.C., Lu, C.W. and Chen, C.Y. (2010), "The carbon distribution in multi-crystalline silicon ingots grown using the directional solidification process", *J. Cryst. Grow*., **312**(8), 1282-1290.

Teng, Y.Y., Chen, J.C., Lu, C.W., Chen, H.I., Hsu, C. and Chen, C.Y. (2011), "Effects of the furnace pressure on oxygen and silicon oxide distributions during the growth of multi-crystalline silicon ingots by the directional solidification process", *J. Cryst. Grow*., **318**(1), 224-229.

Teng, Y.Y. (2011), "Investigation of thermal-fluid and impurity concentration distributions for growing the solar multi-crystalline Si ingots", Ph.D. Dissertation, National Central University, Taiwan.

Teng, Y.Y., Chen, J.C., Huang, C.C., Lu, C.W., Wun, W.T. and Chen, C.Y. (2012), "Numerical investigation of the effect of heat shield shape on the oxygen impurity distribution at the crystal-melt interface during the process of Czochralski silicon crystal growth", *J. Cryst. Grow*., **352**(1), 167-172.

Teng, Y.Y., Chen, J.C., Lu, C.W. and Chen, C.Y. (2012), "Numerical investigation of oxygen impurity distribution during multi-crystalline silicon crystal growth using a gas flow guidance device", *J. Cryst. Grow*., **360**(1), 12-17.

Teng, Y.Y., Chen, J.C., Huang, B.S. and Chang, C.H. (2014), "Numerical simulation of impurity transport under the effect of a gas flow guidance device during the growth of multi-crystalline silicon ingots by the directional solidification process", *J. Cryst. Grow*., **385**(1), 1-8.

Zhang, Z.Q., Huang, Q., Huang, Z.F., Li, B.W. and Chen, X. (2011), "Analysis of microcrystal formation in DS-silicon ingot", *Sci. China*: *Technol. Sci*., **54**(6), 1475-1480.

DC

Nomenclature

C_p	heat capacity, J/kg K
$\bar{g}$	gravity acceleration, m/s^2
k	thermal conductivity, W/m k
n	normal direction of the interface
P	furnace pressure, Pa
q_i^{in}	total radiative flux incoming to the surface i, W/m^2
S	source term
T	Temperature, K
$\bar{u}$	fluid velocity, m/s
ΔH	latent heat, J/kg

Greek letters

ρ	density, kg/m^3
ρ_0	reference density, kg/m^3
$\bar{\tau}$	stress tensor
τ	one of the two orthogonal directions tangential to the interface
μ	dynamic viscosity, Pa *s*
ε	emissivity
σ	Stefan-Boltzmann constant
σ_m	surface tension of the silicon melt, N/m

Subscripts

m	silicon melt
s	silicon crystal